INTERNATIONAL JOURNAL FOR NUMERICAL METHODS IN FLUIDS, VOL. 12, 203–224 (1991)

NUMERICAL ASPECTS OF CALCULATION OF CONFINED SWIRLING FLOWS WITH INTERNAL RECIRCULATION

F. DURST AND D. WENNERBERG*

Lehrstuhl für Strömungsmechanik, Cauerstrasse 4, D-8520 Erlangen, F.R.G.

SUMMARY

Predictions were performed for two different confined swirling flows with internal recirculation zones. The convection terms in the elliptic governing equations were discretized using three different finite differencing schemes: hybrid, quadratic upwind interpolation and skew upwind differencing. For each flow case, calculations were carried out with these schemes and successively refined grids were employed. For the turbulent flow case the k–ε turbulence model was used. The predicted cases were a laminar swirling flow investigated by Bornstein and Escudier, and a turbulent low-swirl case studied by Roback and Johnson. In both cases an internal recirculation zone was present. The laminar case is well predicted when account is taken of the estimated radial velocity component at the chosen inlet plane. The quadratic upwind interpolation and skew upwind schemes predict the main features of the internal recirculation zone also with a coarse grid. The turbulent case is well predicted with the coarse as well as the finer grids, the skew upwind and quadratic upwind interpolation schemes yielding results very close to the measurements. It is concluded that the skew upwind scheme reaches grid independence slightly before the quadratic upwind scheme, both considerably earlier than the hybrid scheme.

KEY WORDS Confined flow Swirling flow k–ε Model predictions

1. INTRODUCTION

Swirling flows are often found in industrial flow applications when intense mixing between different streams is required. A typical example of an application is a swirl-stabilized flame, where an internal recirculating zone acts as a flame holder. Such flows are also of interest in cyclones, where particles are separated from a fluid owing to centrifugal forces imparted by the swirling motion of the flow.

The appearance of an internal recirculation zone on or parallel to the axis of symmetry is typical for these types of flows. Extensive research has been done in order to investigate the basic mechanisms behind the formation of such zones. The works of Benjamin,[1,2] Faler and Leibovich,[3,4] Leibovich[5] and Escudier and Zehnder[6] are all concerned with the mechanisms in the flow which cause these recirculation zones and classification of these in types and forms by flow characteristics. The appearance of these recirculation zones is a sign of the so-called vortex

* Present address: Batelle Europe, Am Römerhof 35, D-6000 Frankfurt a.M. 90, F.R.G.

0271–2091/91/030203–22$11.00

Received July 1989
Revised February 1990

breakdown phenomenon, in which the flow undergoes a change from one flow state to another[1] owing to an instability of the rotating fluid motion. This change in the flow characteristic can be caused by a disturbance in the flow, which typically may be an expansion of the cross-sectional area of the flow channel.

Modelling of swirling flows has been an area of high interest for many years and the subject of many papers. In a confined swirling flow the appearance of the internal recirculating zone causes the forward flow to divert outwards and around this zone. This implies that with the use of an orthogonal grid system (or rather a system that is not aligned with the streamlines) in calculations of such flows, the flow direction is inclined relative to the grid orientation and is therefore also sensitive to the numerical approximations used to discretize the flow equations. Accurate modelling is important for a correct prediction of the size and strength of the internal recirculation zone, and different combinations of grid fineness and discretization scheme may produce very different results, owing to what is known as numerical diffusion.

More accurate predictions are always achievable by using finer grids. However, there are practical limits to grid refinements owing to the limited size of available computers and to limitations on computer time. For instance, an application to the calculation of swirl-stabilized pulverized fuel flames requires not only the fluid field to be computed but also the energy and different species equations, and the particle motion has to be calculated considering all the couplings between the equations, as done for instance by Wennerberg.[7] In such a complex case the number of grid nodes applied will be restricted even when the most efficient and largest computers are employed. Hence, the use of more accurate differencing schemes will be an advantage if these can give more accurate results with fewer grid points and thus permit computations with the available computer power.

The turbulence model used in swirling flow predictions will of course also have a strong influence on the results. However, in order to estimate the influence of different turbulence models, one has to ascertain that the numerical solution errors are minimized, i.e. the numerical grid used has to be fine enough and the differencing scheme as efficient as possible to yield reliable results.

Comparisons of different finite differencing schemes in isothermal non-swirling recirculating flows were carried out by Leschziner,[8] Leschziner and Rodi,[9] Sharif and Busnaina[10] and Patel *et al.*,[11] among others. Syed *et al.*[12] did a thorough investigation on the efficiency of different differencing schemes in both two and three dimensions with applications to swirling combustor flows. Their conclusions were that higher-order schemes give better accuracy than hybrid or upwind schemes, but that the accuracy of the different higher-order schemes is dependent on the flow angle. Syed *et al.* recommended a bounded variant of skew upstream differencing. Sturgess and Syed[13] applied some of these investigated schemes to some swirling flow cases and pointed out the importance of numerical accuracy. Higher-order schemes (QUICK) have been used, for instance, by Nikjooy,[14] Rhode and Stowers[15] and Weber *et al.*[16] for calculation of swirling flows, but no direct comparisons of the influence of different differencing schemes or grid fineness were given.

The objective of the work presented here was to compare different discretizing methods for the equations of motion applied to swirling flows with internal recirculation zones. Comparisons were made for two different cases where experimental data were also available. Calculations were performed with the above-mentioned differencing schemes and finer and coarser grids were employed for all schemes. In Section 2 the governing equations are presented as well as the different methods used for discretizing these into finite difference equations. In Section 3 the available experimental data to be used for the test calculations are discussed and in Section 4 the results of the predictions are presented and discussed for the different cases.

Table I. Source term expressions for the independent variables in equation (1), and constants in the turbulence model

Variable	Φ	Source term	Γ_{eff}
Mass	1	—	0
Axial momentum	u	$\frac{\partial}{\partial x}\left(\Gamma_{eff}\frac{\partial \bar{u}}{\partial x}\right)+\frac{1}{r}\frac{\partial}{\partial r}\left(\Gamma_{eff}\, r\frac{\partial \bar{v}}{\partial x}\right)-\frac{\partial \bar{p}}{\partial x}$	μ_{eff}
Radial momentum	v	$\frac{\partial}{\partial x}\left(\Gamma_{eff}\frac{\partial \bar{u}}{\partial r}\right)+\frac{1}{r}\frac{\partial}{\partial r}\left(\Gamma_{eff}\, r\frac{\partial \bar{v}}{\partial r}\right)-\frac{\partial \bar{p}}{\partial r}-2\Gamma_{eff}\frac{\bar{v}}{r^2}+\frac{\rho \bar{w}^2}{r}$	μ_{eff}
Angular momentum	w	$-\frac{\rho \bar{v}\bar{w}}{r}-\frac{\bar{w}}{r^2}\frac{\partial}{\partial r}(r\Gamma_{eff})$	μ_{eff}
Turbulent kinetic energy	k	$G_k-\rho\varepsilon$	μ_{eff}/σ_k
Dissipation rate of turbulence energy	ε	$\frac{\varepsilon}{k}(C_1 G_k-C_2\rho\varepsilon)$	$\mu_{eff}/\sigma_\varepsilon$

where

$$G_k=\mu_{eff}\left\{2\left[\left(\frac{\partial \bar{u}}{\partial x}\right)^2+\left(\frac{\partial \bar{v}}{\partial r}\right)^2+\left(\frac{\bar{v}}{r}\right)^2\right]+\left(\frac{\partial \bar{w}}{\partial x}\right)^2+\left[r\frac{\partial}{\partial r}\left(\frac{\bar{w}}{r}\right)\right]^2+\left(\frac{\partial \bar{u}}{\partial r}+\frac{\partial \bar{v}}{\partial x}\right)^2\right\}$$

$$\mu_{eff}=C_\mu\rho\frac{k^2}{\varepsilon}$$

Constants	C_μ	C_1	C_2	σ_k	σ_ε
	0·09	1·44	1·92	1·0	1·3

2. CALCULATION PROCEDURES

2.1. Governing equations for axisymmetric swirling flow

The general form of the elliptic differential equations governing an axisymmetric swirling flow can be expressed as (see e.g. Khalil[17])

$$\frac{\partial}{\partial x}(\rho \bar{u}\bar{\Phi})+\frac{1}{r}\frac{\partial}{\partial r}(\rho r\bar{v}\bar{\Phi})-\frac{\partial}{\partial x}\left(\Gamma_{eff}\frac{\partial \bar{\Phi}}{\partial x}\right)-\frac{1}{r}\frac{\partial}{\partial r}\left(r\Gamma_{eff}\frac{\partial \bar{\Phi}}{\partial r}\right)=S_\Phi, \tag{1}$$

where x is the co-ordinate in the main flow direction, r is the radial co-ordinate, ρ is the fluid density and $\bar{u}$ and $\bar{v}$ are the velocity components in the x- and r-directions respectively. S_Φ is the source term and Γ_{eff} is the effective viscosity or diffusivity for the different variables Φ as given in Table I. The standard procedure for converting this equation into a finite difference equation is to integrate it over a control volume and evaluate the respective fluid properties at control volume boundaries.[17] The diffusion terms are naturally treated with central differencing, since the derivative is evaluated on the border between two adjacent control volumes, i.e. at point w, e, n or s in Figure 1.

For evaluation of the convective terms, the variable Φ has to be estimated on the boundary of the control volume; see Figure 1. It is in this respect that the differencing schemes used here differ from one another.

2.1.1. Hybrid differencing. The standard method for differencing the convection terms is the so-called hybrid differencing, where central differencing for the convection terms is used for cell Peclet numbers less than 2 and upwind differencing for higher Peclet numbers, i.e. the value is taken at point W, E, N or S in Figure 1, depending on the flow direction. As is well known, this practice always gives positive coefficients in the difference equations and is therefore always numerically stable.

However, this scheme is known to be less accurate when the flow direction is not aligned with the orientations of the surface vectors of the control volumes. These inaccuracies are referred to as numerical diffusion, emanating from the fact that a rigorous error estimate for the discretized equations results in second-derivative, i.e. diffusion-like, terms. This error can be shown to be maximum when the flow angle relative to the control volume alignment is 45°.[12]

2.1.2. Skew upwind differencing. The skew upwind differencing scheme was proposed by Raithby.[18] Here the convected property on the boundary is interpolated over the cell face, taking the flow *vector* in the upstream direction into account. That implies that the SW, NW, SE and NE points are also introduced into the differencing scheme (see Figure 1), which will decrease the effect of numerical diffusion as described above. Error estimates for different flow angles and different test cases are given by Syed *et al.*[12]

For this scheme, however, the coefficients of the resultant solution matrix may become negative, which can lead to instabilities and convergence problems. This may be improved by using flux blending, i.e. the convective flux can be calculated as a weighted sum of the flux expressions from the upwind and skew upwind differencing schemes, as proposed by Syed *et al.*[12] or Peric *et al.*[19] By lowering the weighting factor, the flux is calculated with more weight from the

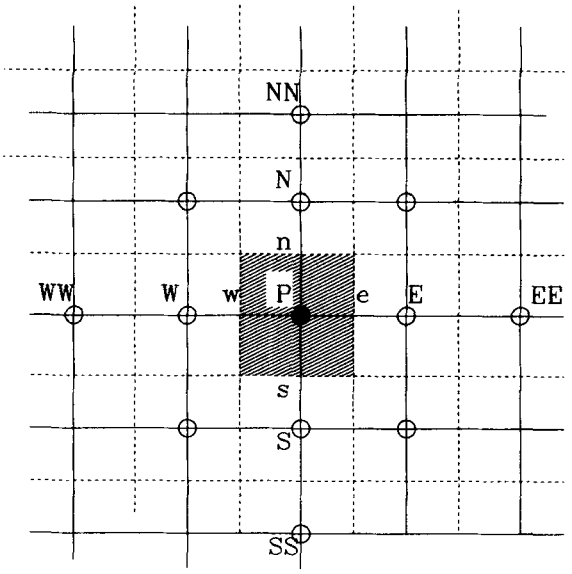

Figure 1. Grid alignment and node points used in the differencing schemes

pure upwind scheme and therefore given more positive influence coefficients at the cost of more numerical diffusion. This procedure was used in the calculations presented here. The weighting factors have been taken as constants here for reasons of simplicity; various optimization schemes for local values of the weighting factors may also be derived.[12]

2.1.3. QUICK differencing scheme. The quadratic upstream interpolation differencing scheme was proposed by Leonard.[20] The basic principle behind this scheme is the utilization of three points in the upstream direction for evaluation of the cell face convected property, i.e. the points WW, EE, NN or SS are included (see Figure 1), depending on the flow direction. A quadratic expression involving three points in a line is used for evaluating the cell face property.

The influence coefficients may also become negative as for the skew upwind scheme. However, there are possibilities to manipulate the discretized equations in order to always achieve positive coefficients in the coefficient matrix, as done by Pollard and Siu.[21] Their formulation gives slower convergence though, since they put some of the dominating terms into the source term. In the present work another formulation, proposed by Shyy,[22] was used which gives a coefficient matrix that is more diagonally dominant than Pollard and Siu's formulation. In addition to that, the flux-blending technique described above was also employed and fully implemented into the QUICK scheme.

2.1.4. Solution procedure. A modified version of the well-known TEACH code with a staggered grid arrangement was used for all the predictions carried out in this study. The SIMPLE procedure[23] with proper relaxation factors[19] was used for the pressure–velocity coupling. For the solution of the resulting tridiagonal coefficient matrix system, Stone's algorithm[24] was employed for the pressure correction equation and Stone's algorithm or TDMA was used for the other equations.

There were essentially no severe convergence problems encountered for the cases predicted here, neither for the skew upwind nor the QUICK differencing schemes. Only for the laminar flow case and for the QUICK scheme did the flux-blending weighting factors have to be lowered to 0·6 for the fine grid cases to yield converged solutions. Relaxation factors were of the order of 0·5–0·6 or higher. The iterations were continued until the residuals for velocities and mass conservation were smaller than 5×10^{-3}, also for the finer grids. The two higher-order schemes required more iterations to achieve convergence, and they required approximately 15%–20% and 35%–40% more computing time per iteration for QUICK and skew upwind respectively.

2.2. Turbulence modelling

The predictions for the turbulent flow case were performed with the so-called k–ε model. This model is usually not considered to be fully suitable for turbulent flows with strong swirl. The objectives in this work, however, were not primarily to evaluate the turbulence model but rather to assess the influence of the numerical aspects of discretization and grid fineness on the prediction of swirling flows with internal recirculation. The results from the low-swirl case indicate that the k–ε model yields sufficiently accurate predictions of the mean flow properties.

The same differencing schemes were used for the k- and ε-equations as for the three momentum equations. It may, however, be argued that in the regions where the flow is at a large angle to the grid system, i.e. at the outer edges of the recirculation zone, the turbulence production terms are probably large in comparison with convective transport and therefore numerical diffusion may be less important in the k- and ε-equations. It was also noted that the same partly applies to the tangential velocity momentum equation, which sometimes also contains dominating source terms; see Table I.

3. DATA FOR MODEL EVALUATION

Evaluation of the efficiency of the different differencing schemes may be studied by successive refinement of the grid. In general and for complex flow systems this approach may not be feasible, however, owing to limitations in computer storage and availability of computer time. However, for the achieved computational accuracy it is not only the total number of grid points utilized that is of interest but also their distribution over the computational domain. What matters in the end is of course the closeness of the predictions to the corresponding measurements. Here, assessment of computational accuracy was done by comparing the computational results for increasingly refined numerical grids as well as comparing the results with measurements.

Sloan *et al.*[25] carried out a review of experimental data on confined swirling flows. They reviewed 100 references on this type of flow for use as evaluation data for swirling flow prediction procedures. Their considerations included measurement quality and accuracy, availability of data, recency of study, etc. Of all the considered papers, only a small number, approximately 10, were considered by Sloan *et al.* to be sufficiently recent, accurate and available in suitable form to be compared with numerical predictions.

On the basis of the work of Sloan *et al.*, two different cases[26,27] were chosen for use as test cases here. The flow characteristics of these two flows are summarized in Table II and the test section geometries are shown in Figure 2. The two cases are a laminar low-swirl flow[26] and a turbulent low-swirl flow.[27] In both cases there is an internal recirculation zone formed which forces the forward flow outwards towards the confinement walls and thus causes the flow to be at an angle to the symmetry axis. Both cases should therefore be sensitive to the effects of numerical diffusion.

Inlet conditions were only partly available for the two cases. LDV measurements of the axial and tangential velocities, and in the case of the turbulent flow also the main strains in the three co-ordinate directions, were available for the cases considered here. However, in neither of the cases could the measured inlet conditions be used directly without modification to get the inlet conditions for the predictions. The necessary modifications for each case will be described below. One point that should be mentioned here is the importance of also measuring the radial velocity component at the inlet in swirling flows. Owing to the rotating motion imparted by the swirl element used, a radial velocity component will necessarily develop downstream of the swirler. This becomes apparent from looking at the geometry of the test sections in Figure 2.

Test case 1 is a laminar swirling flow case measured by Bornstein and Escudier.[26] Their flow geometry is shown in Figure 2(a). In their study the swirler consisted of radial inflow vanes from where the flow entered the flow tube. An insert acted as a step expansion, which provided the necessary disturbance to cause vortex breakdown and the creation of an internal recirculation zone. The case presented by Bornstein and Escudier represents a flow with a Reynolds number of 612 and a swirl number of 0·34; see Table II. Measurements of the axial and tangential velocity components were carried out by the authors at several stations downstream of the expansion step. The mass balance from the LDV measured profiles yielded flow rate results to $\pm 5\%$ within the given mass flow rate.

The first measured profile was taken 7 mm downstream of the expansion step; see Figure 2(a). Therefore the inlet conditions had to be derived from data extrapolated upstream to the expansion plane. From the data in Reference 26 it is evident that there was a radial velocity component present in the flow already at the expansion plane. The flow exited from the radial vane swirler and developed in the short insert tube (83 mm), and owing to the swirling motion and the 90° bend, the pressure field imposed a radial velocity component on the flow. As will be seen from the results of the predictions for this case, this radial component is of utmost importance in yielding the final predicted flow results. For the present predictions the radial velocity component could be estimated from the streamfunction at the first measuring plane, constructed from

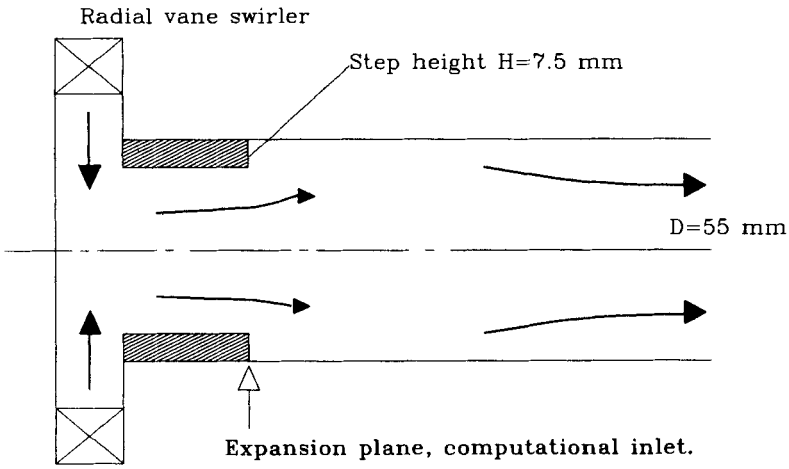

Figure 2(a). Geometry of Bornstein/Escudier test section

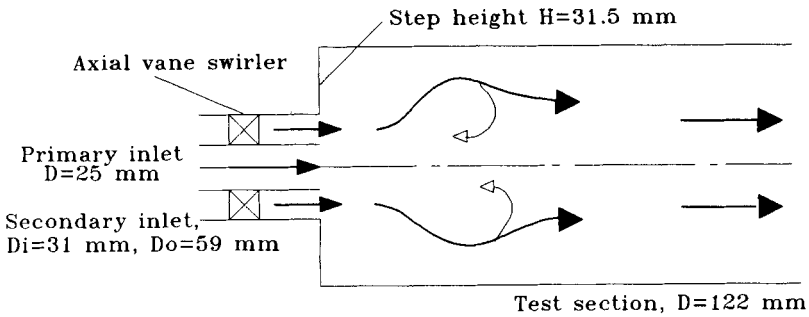

Figure 2(b). Geometry for Roback/Johnson case

Table II. Flow characteristics for the two test cases

Reference	Swirl number	*Re*	Inlet velocity ($m\ s^{-1}$)	Fluid
Bornstein and Escudier[26]	0·34	612	0·02	Water
Roback and Johnson[27]	0·38	47000	0·53/1·67	Water

measured axial velocities, and then extrapolated upstream to the expansion plane where the calculations were started. The radial velocity component was estimated in this way to be of the order of 10%–15% of the axial velocity component.

The second test case represents the flow in the test section of Figure 2(b) and is based on the measurements of Roback and Johnson[27] in a confined double-concentric jet with a sudden expansion; see Figure 2(b). In their study the swirler was an axial vane swirler placed in the secondary annular inlet and the swirl number was 0·38; see Table II. Extensive measurements of mean quantities and main strains in the three co-ordinate directions and all three stress

components, performed with a two-component LDV system, were carried out by Roback and Johnson. The integrated mass flow from LDV-measured profiles was within 10%–15% of the given total mass flow rate. However, also for this study the first measuring plane was slightly downstream (5 mm) of the expansion plane and hence was sufficiently distant to have already caused an expansion of the flow. This can readily be deduced from the first measured velocity profile. However, enough measurements of the radial velocity are provided at this plane to deduce further flow information. The radial velocity components estimated in this way at the expansion plane are of the order of a few per cent of the axial velocity components for this flow case, i.e. of less importance for the development of the flow, in contrast to test case 1. This is readily explainable, since an axial vane swirler in an annulus should be a more favourable flow configuration in this respect than the swirl generator in test case 1.

4. RESULTS AND DISCUSSION

4.1. Test case 1, laminar flow, Bornstein/Escudier

As already mentioned above, the calculations for test case 1 were started at the step expansion plane (see Figure 2(a)) with the axial and tangential velocity profiles from Bornstein and Escudier's first measuring position, but extrapolated upstream by about 7 mm. In this way the inlet boundary conditions were obtained and the outlet boundary conditions were set sufficiently distant from the recirculation region in the flow. Calculations were performed with three different non-uniform grids: a coarse with 36×30 nodes and two finer grids with 70×58 and 138×114 nodes. The finer grids were obtained by successively reducing the coarser grid spacings to half the size.

Calculations were first performed with only the axial and tangential velocities given at the inlet, i.e. with the radial component equal to zero. This resulted in a flow without internal recirculation and with positive velocities at all axial locations near the centreline. This is also consistent with the results reported by Sloan *et al.*,[25] who were also unable to predict flow reversal in the central parts of this flow. Sloan *et al.* also carried out predictions with a very fine grid (95×94) without seeing any flow reversal. Hence the present study is consistent with this finding.

However, as discussed in Section 3 above, it is evident that the flow contains a radial velocity component already at the expansion plane. An estimate of the magnitude of this could be achieved from the streamfunction, calculated from the axial velocity component data at the first measuring positions in the Bornstein/Escudier experiment. This resulted in a distribution of the radial velocity component providing an overall magnitude of up to 15% of the axial velocity component. The extended data, with non-zero radial velocity components, were then used as inlet conditions for the following predictions.

Figures 3(a) and 3(b) show the predicted flow field with the finest grid and calculated with the QUICK differencing scheme. In the lower half of Figure 3(b) the streamlines calculated from the Bornstein/Escudier measurements are shown. It is seen that the main features of the 'vortex breakdown bubble' are very well predicted. The stagnation point in the Bornstein/Escudier experiment was 20 mm downstream of the expansion plane, which is very well predicted here, as is the overall form of the recirculation zone. However, in the predictions the length of the toroidal part extends to approximately 70 mm downstream of the expansion plane whereas in the measurements it extended down to approximately 95 mm.

Figure 3(c) shows the same comparison for the predictions carried out with the skew upwind differencing scheme, also with the finest grid. The stagnation point is shifted slightly upstream, otherwise the results are almost identical.

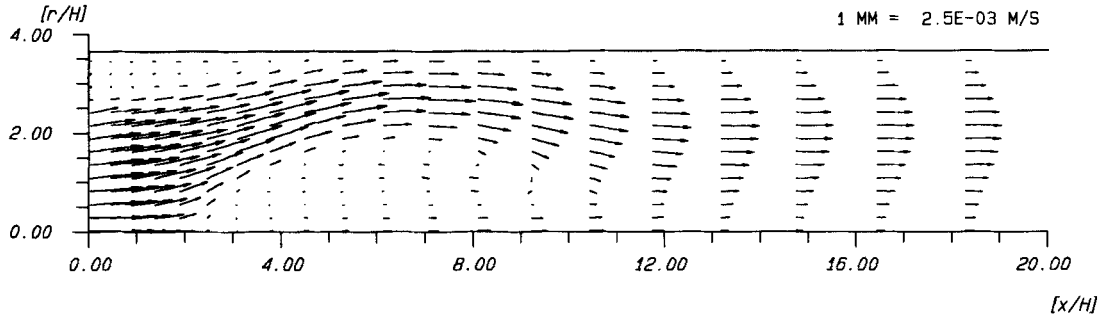

Figure 3(a). Velocity vectors; Bornstein/Escudier laminar flow, QUICK scheme, 138 × 114 grid

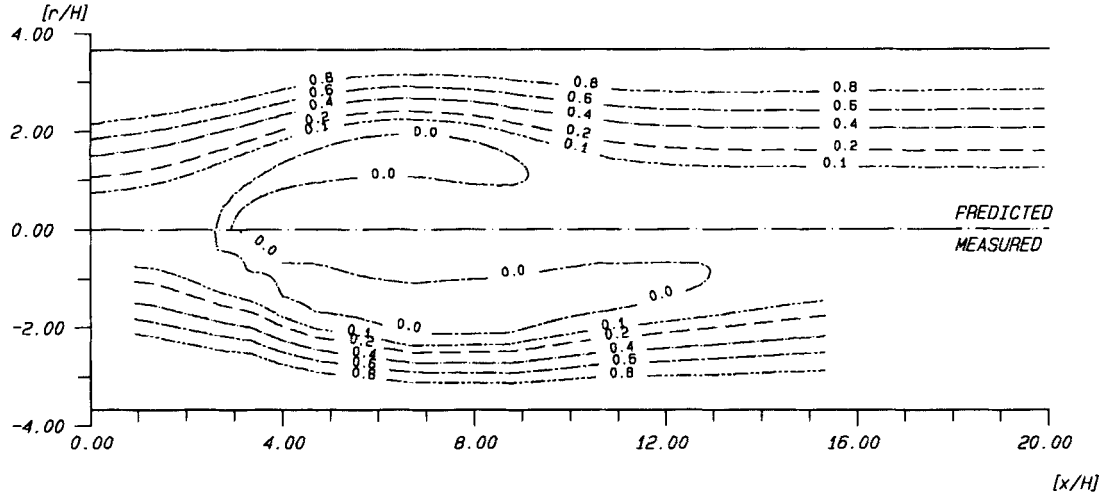

Figure 3(b). Streamlines; Bornstein/Escudier, QUICK differencing, 138 × 114 grid

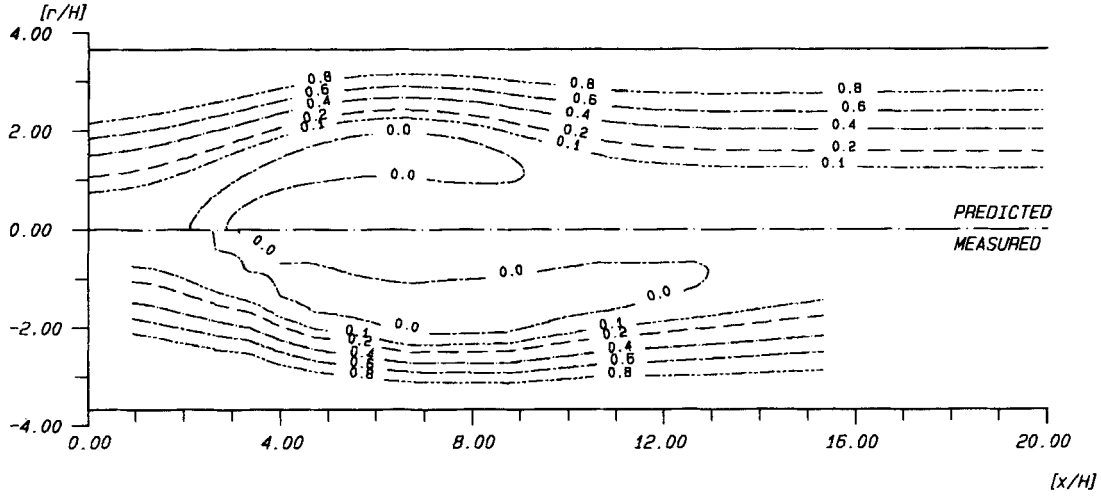

Figure 3(c). Streamlines; Bornstein/Escudier, skew upwind differencing, 138 × 114 grid

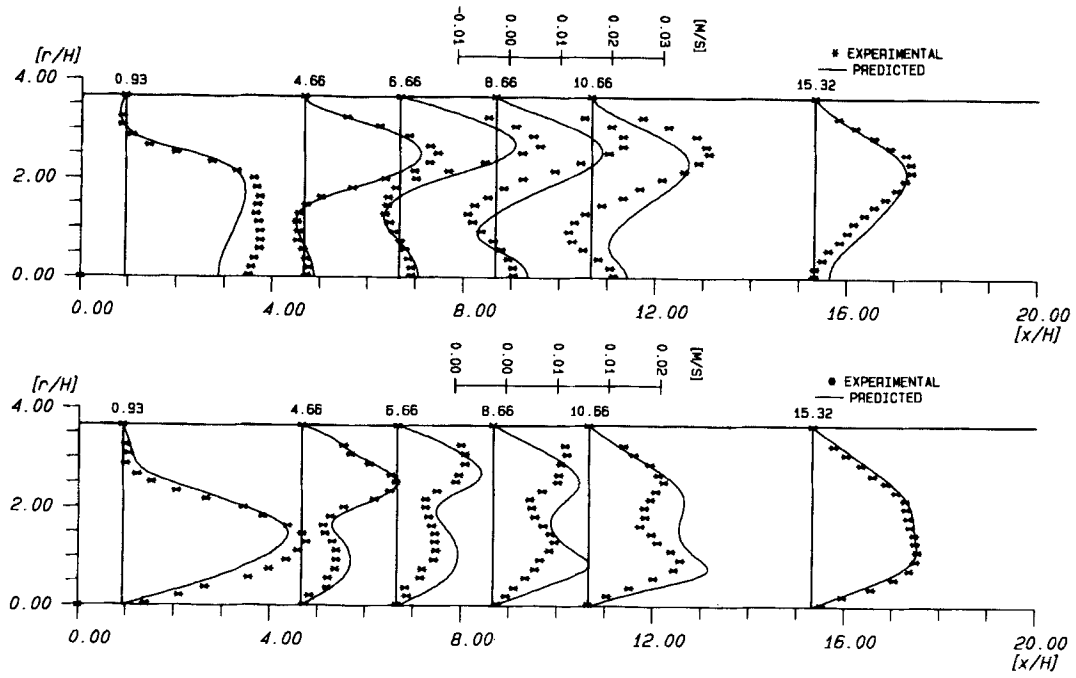

Figure 4(a). Axial (top) and tangential (bottom) velocity profiles; Bornstein/Escudier, QUICK scheme, 138 × 114 grid

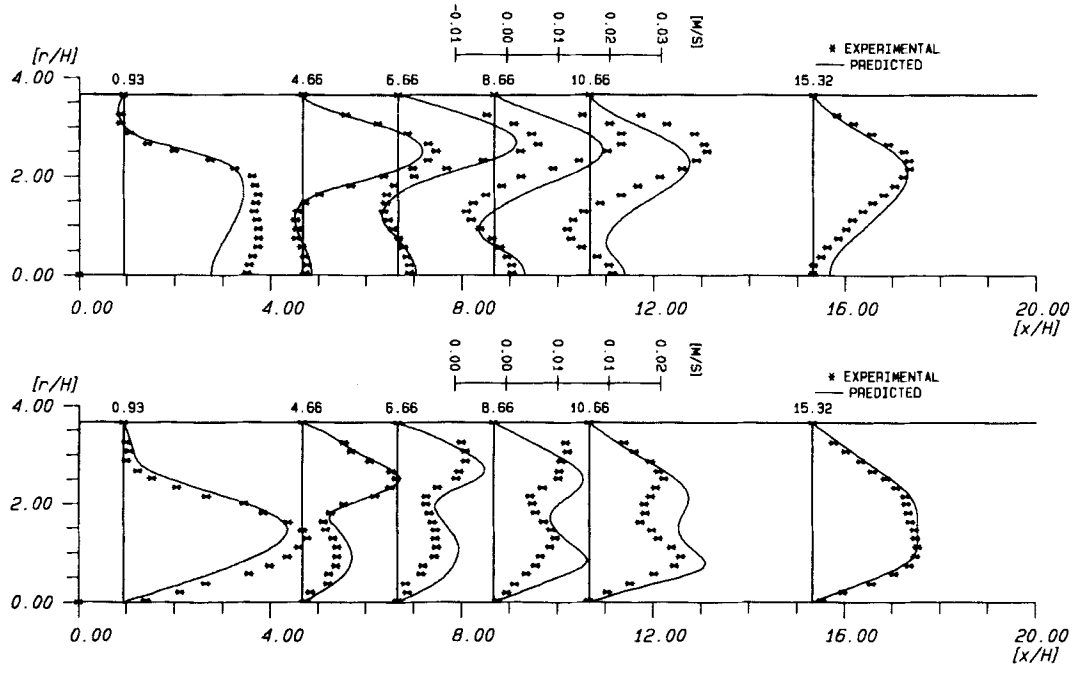

Figure 4(b). Axial (top) and tangential (bottom) velocity profiles; Bornstein/Escudier, skew upwind scheme, 138 × 114 grid

In Figures 4(a) and 4(b) the axial and tangential velocity profiles obtained by the QUICK and skew upwind differencing schemes respectively are compared with the measured profiles. The slopes of the profiles are well predicted, including the double humps of the tangential velocity profiles due to the upstream transport of tangential momentum. The profiles at the first axial location (7 mm) indicate too high an outward shift, probably owing to too high an estimated radial velocity at the expansion plane. However, it was felt that the only reasonable estimate of the radial velocity was to use the recalculated values from the measured streamfunction. Therefore these values were used for all calculations.

In Figures 5 and 6 the predicted streamlines in the sensitive region of the flow are compared, i.e. in the toroidal recirculation zone, and results are given for the different discretization schemes and for different grid sizes. On the left-hand side of Figure 5 the predictions with the coarser grid (36×30) are shown in the following order: at the top the hybrid, then the skew upwind and at the bottom the QUICK differencing scheme. Both the skew upwind and QUICK schemes are also able to resolve the toroidal form of the recirculation zone with the coarse grid, in contrast to the hybrid scheme which fails to do so. The differences between the results of the various differencing schemes are smaller with the medium-size grid (70×58), the QUICK scheme being closest to the measured recirculation zone form. Figure 6 shows the same comparison between the finer grids (70×58 and 138×114). The differences diminish with grid fineness as expected. The QUICK scheme seems remarkably little influenced by the grid fineness, the results being almost identical for the finer and the coarse grids, and the prediction for the coarse grid is already close to the experimental data.

In Figure 7 the relative differences in axial velocity between the predictions with coarse and finer grids for the different finite differencing schemes are shown. The finer-grid results were linearly interpolated back onto the next coarser grid with double the grid line spacing, and the difference between the two values normalized with inlet velocity. It can be seen from Figure 7 that the changes are essentially smaller for the QUICK and skew upwind schemes than for the hybrid scheme and that the differences are concentrated around the boundary regions between forward and backward flow. The hatched areas in Figures 7 and 8 indicate a difference of 20%, given the described normalization. It may be concluded that the skew upwind scheme approaches grid independence faster than the QUICK scheme in this case, as can be seen from Figure 7. This is due to the fact that for the predictions with the QUICK scheme in this case the flux-blending factors had to be lowered to 0·7 and 0·6 respectively for the finer grids from the value 0·85 used for the coarse-grid QUICK scheme computations. The influence of differencing is also felt more in the axial velocity calculations than in the tangential velocity calculations; see Figure 8, where corresponding data are shown for the tangential velocity. This can be explained by looking at the source terms in the respective equations in Table I. The magnitude of the source terms in the angular velocity equation is larger than the axial velocity equation source terms, which makes the solution less dependent on the approximations for the convection terms.

4.2. Test case 2, Roback/Johnson

Predictions of the experiments of Roback and Johnson[27] have been presented by several authors.[12–14,25] Also in this case it is natural to start calculations at the expansion plane, even though the first measuring position was taken 5 mm downstream of the expansion in Roback and Johnson's experiment. To predict this flow, the measured axial and tangential velocity profiles at 5 mm were slightly adjusted near the edges and used as inlet conditions at the expansion plane. Measurements of all three main strains were used to calculate inlet values for the turbulence

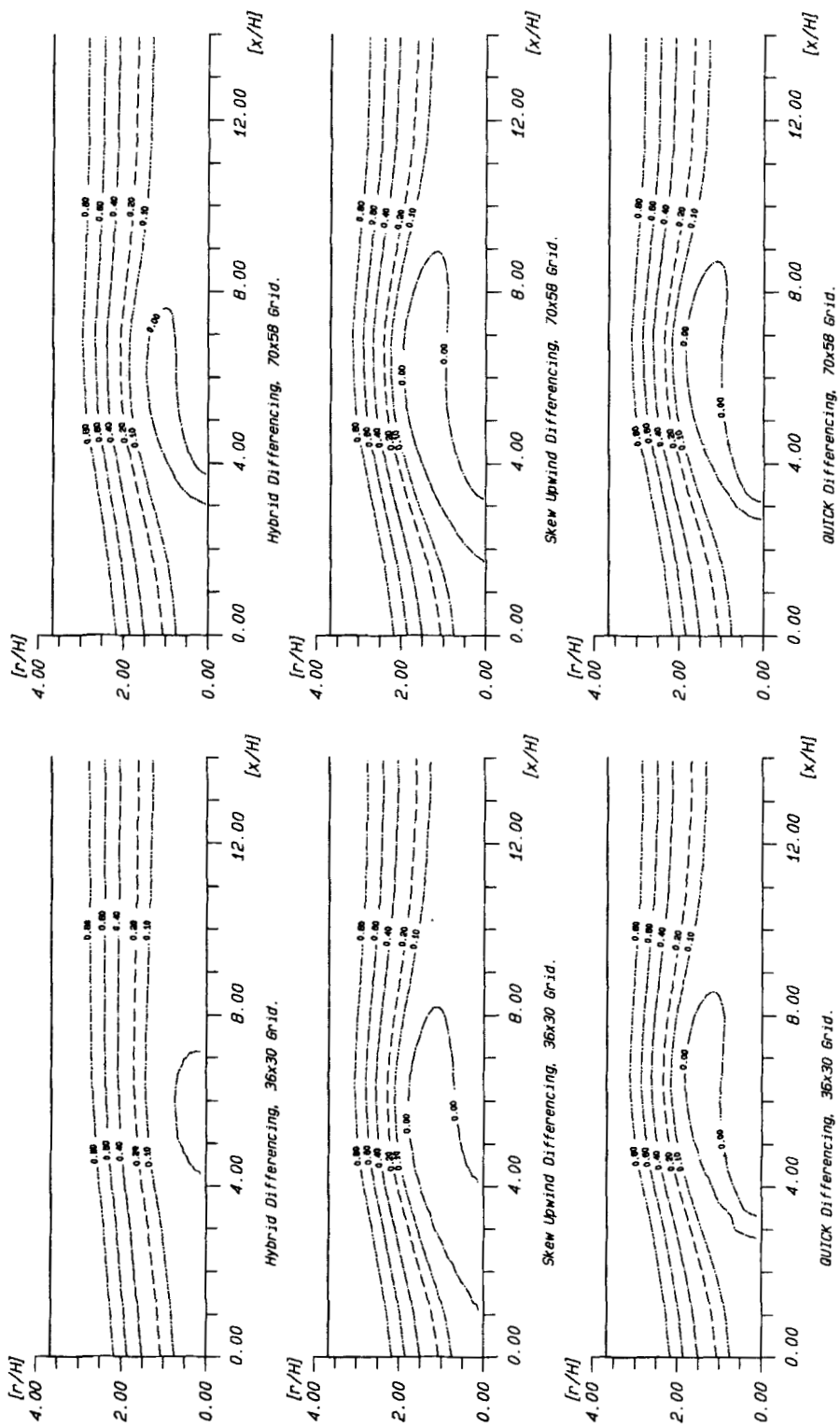

Figure 5. Comparison of recirculation zone extension for the coarser grids; Bornstein/Escudier case

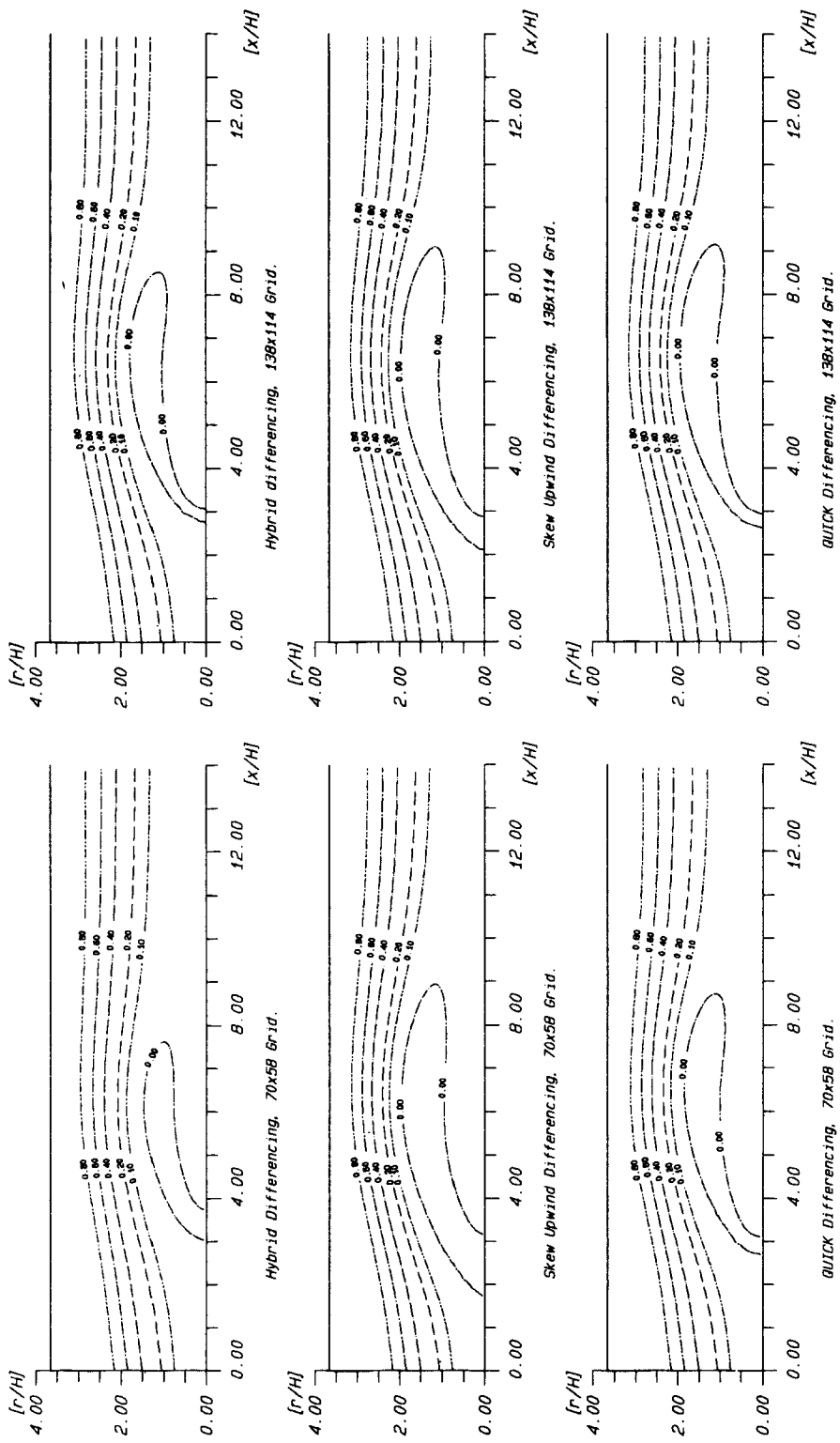

Figure 6. Comparison of recirculation zone extension for the finer grids; Bornstein/Escudier case

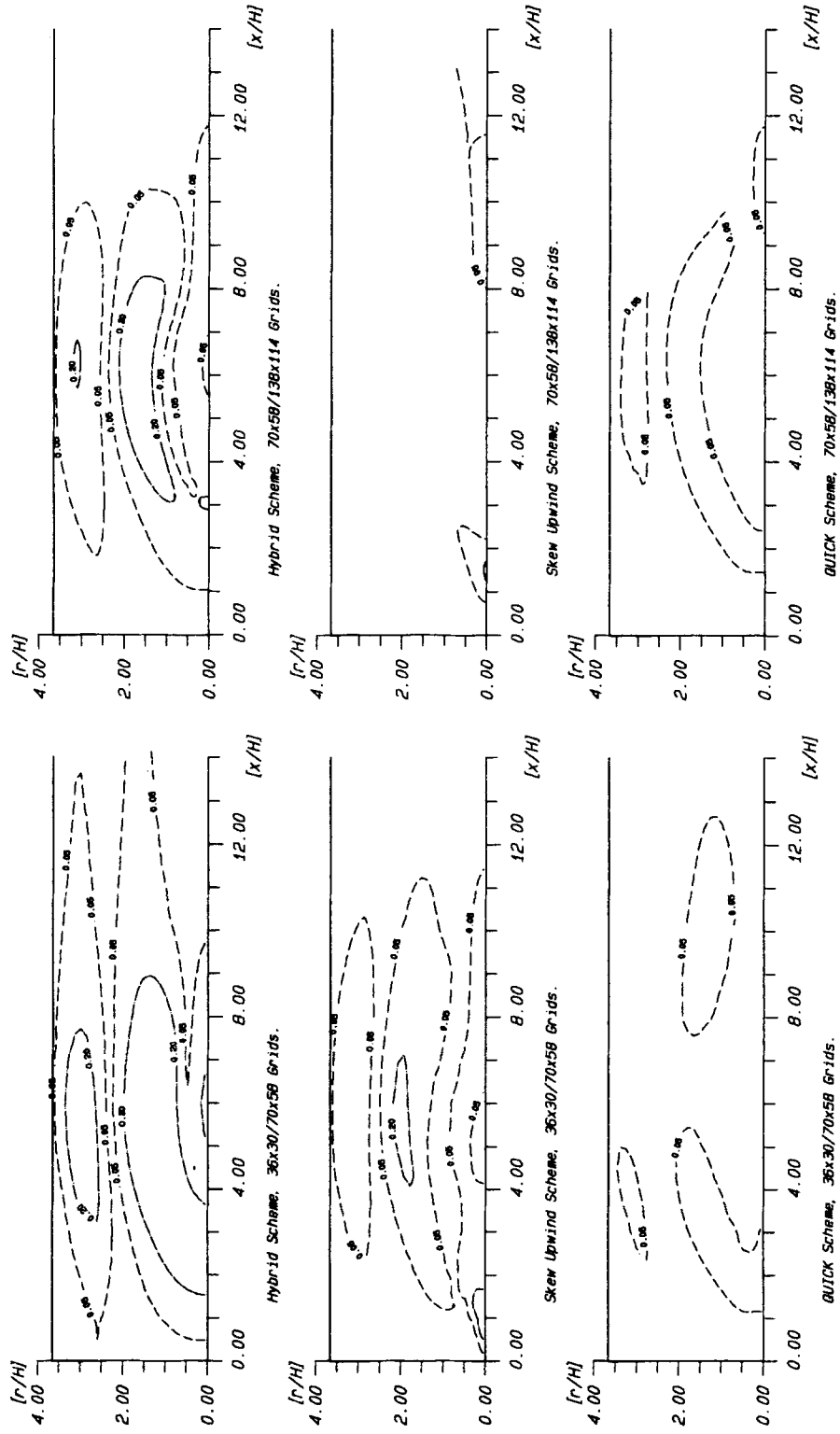

Figure 7. Comparison of error estimates for axial velocities: left, 36 × 30/70 × 58 grids; right, 70 × 58/138 × 114 grids

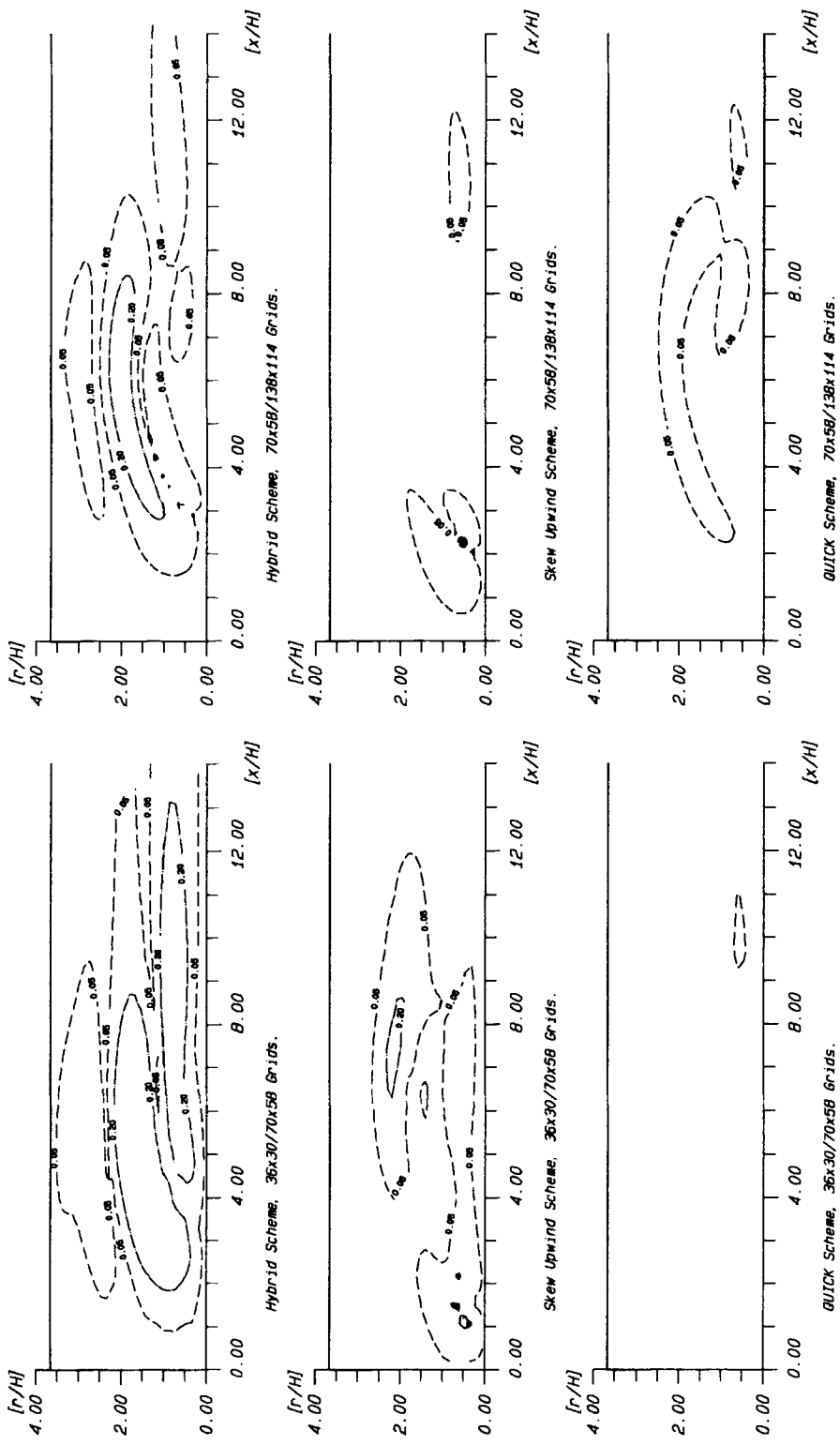

Figure 8. Comparison of error estimates for tangential velocities: left, 36 × 30/70 × 58 grids; right, 70 × 58/138 × 114 grids

energy. Dissipation was estimated from the expression

$$\varepsilon = C_\mu k^{1.5}/l_m, \tag{2}$$

with

$$l_m = 0{\cdot}03\Delta y.$$

The radial velocity was also set to zero at the secondary inlet, in agreement with the discussion in Section 3. Predictions were performed with three different non-uniform grids, consisting of 40×39, 78×76 and 154×150 nodes, again providing successive doubling of the grid densities.

An overview of the predicted flow is given in Figure 9(a), where velocity vectors are shown. A closed internal recirculation zone is formed in the centre of the flow, with an additional

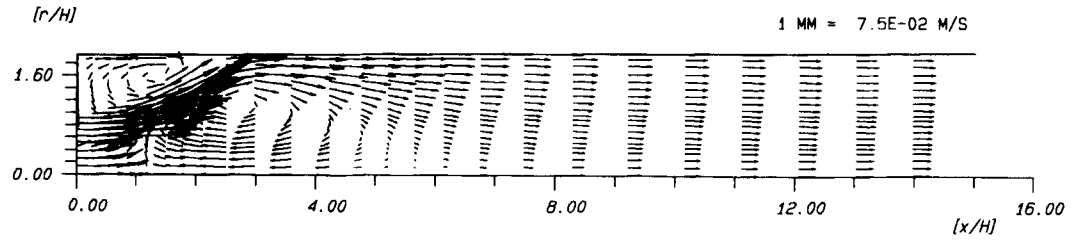

Figure 9(a). Velocity vectors; Roback/Johnson, QUICK scheme, 154×150 grid

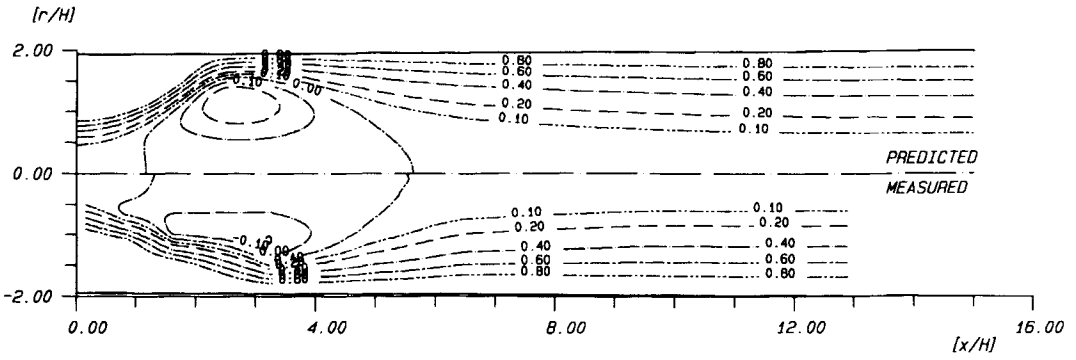

Figure 9(b). Streamlines; Roback/Johnson, QUICK differencing, 154×150 grid

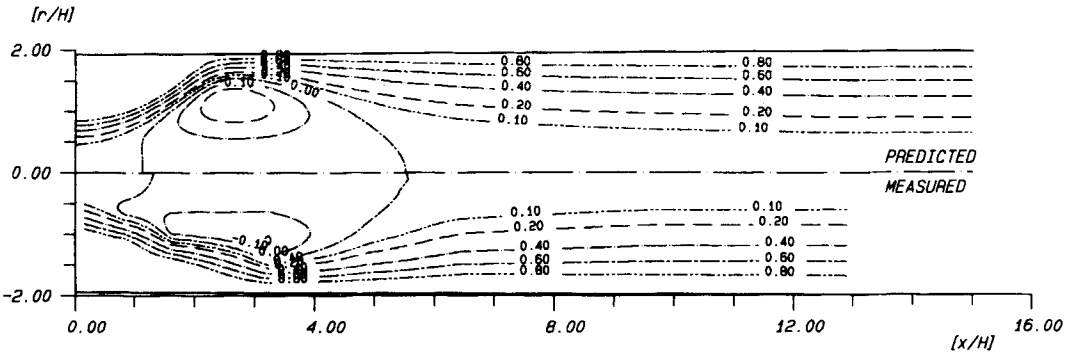

Figure 9(c). Streamlines; Roback/Johnson, skew upwind differencing, 154×150 grid

recirculation zone at the corners downstream of the step (Figure 9(b)). This causes a flow diversion outwards with high gradients in between these two zones and streamlines inclined to the main flow direction (Figure 9(a)). Streamlines predicted with the QUICK scheme and the finest grid (top), and Roback and Johnson's measured (bottom) streamlines are compared in Figure 9(b). The recirculation zone is very well predicted in form and extension; only the primary jet penetration in the initial part is slightly underestimated.

The prediction with the skew upwind differencing scheme for the same case results in almost identical conditions; see Figure 9(c). Comparisons of measured and predicted axial and tangential velocity profiles and turbulence intensity are shown in Figure 10, with details of the first five profile positions given in Figure 11. The agreement with the experimental data is good for the velocities for all three differencing schemes (Figure 11). The only discrepancy is the developed shape of the tangential velocity profiles (Figure 10). In the predictions they tend to adjust towards a free vortex flow, whereas in the measurements it is a forced vortex type of flow. Of the other predictions for this flow, e.g. see References 12, 13, 15 and 25, only Nikjooy[14] reports predicted profiles for the developed shape of the tangential velocity close to the experimental data; they were carried out with an algebraic and a Reynolds stress model. Nevertheless, it seems that the k–ε model is able to predict the mean flow properties in this case with an accuracy sufficient for

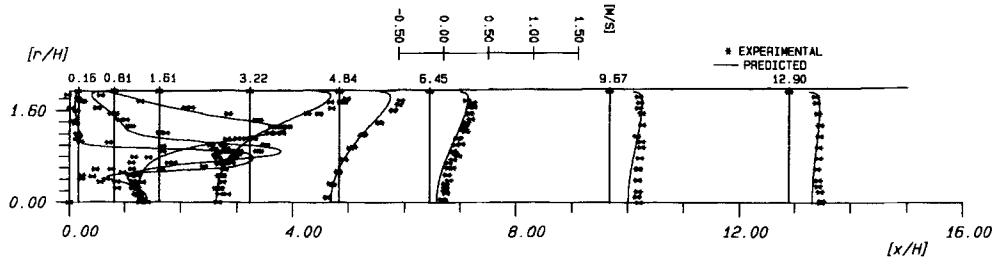

Figure 10(a). Axial velocity profiles; Roback/Johnson, skew upwind scheme, 154 × 150 grid

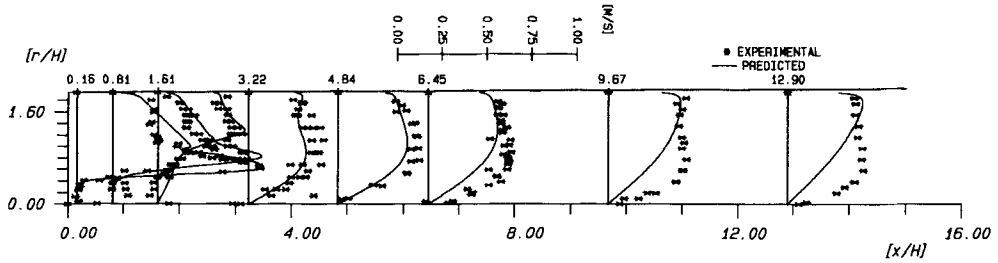

Figure 10(b). Tangential velocity profiles; Roback/Johnson, skew upwind scheme, 154 × 150 grid

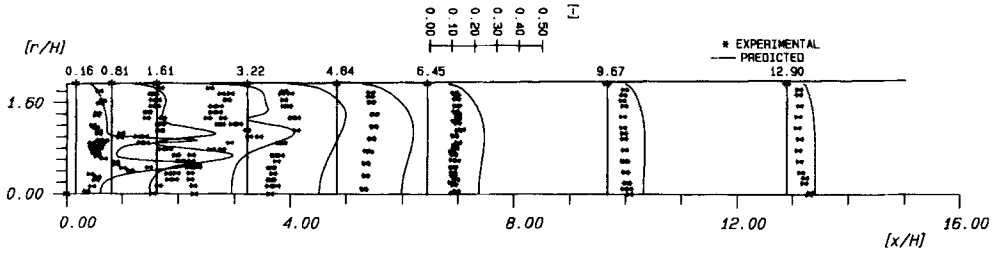

Figure 10(c). Turbulence intensity profiles; Roback/Johnson, skew upwind scheme, 154 × 150 grid

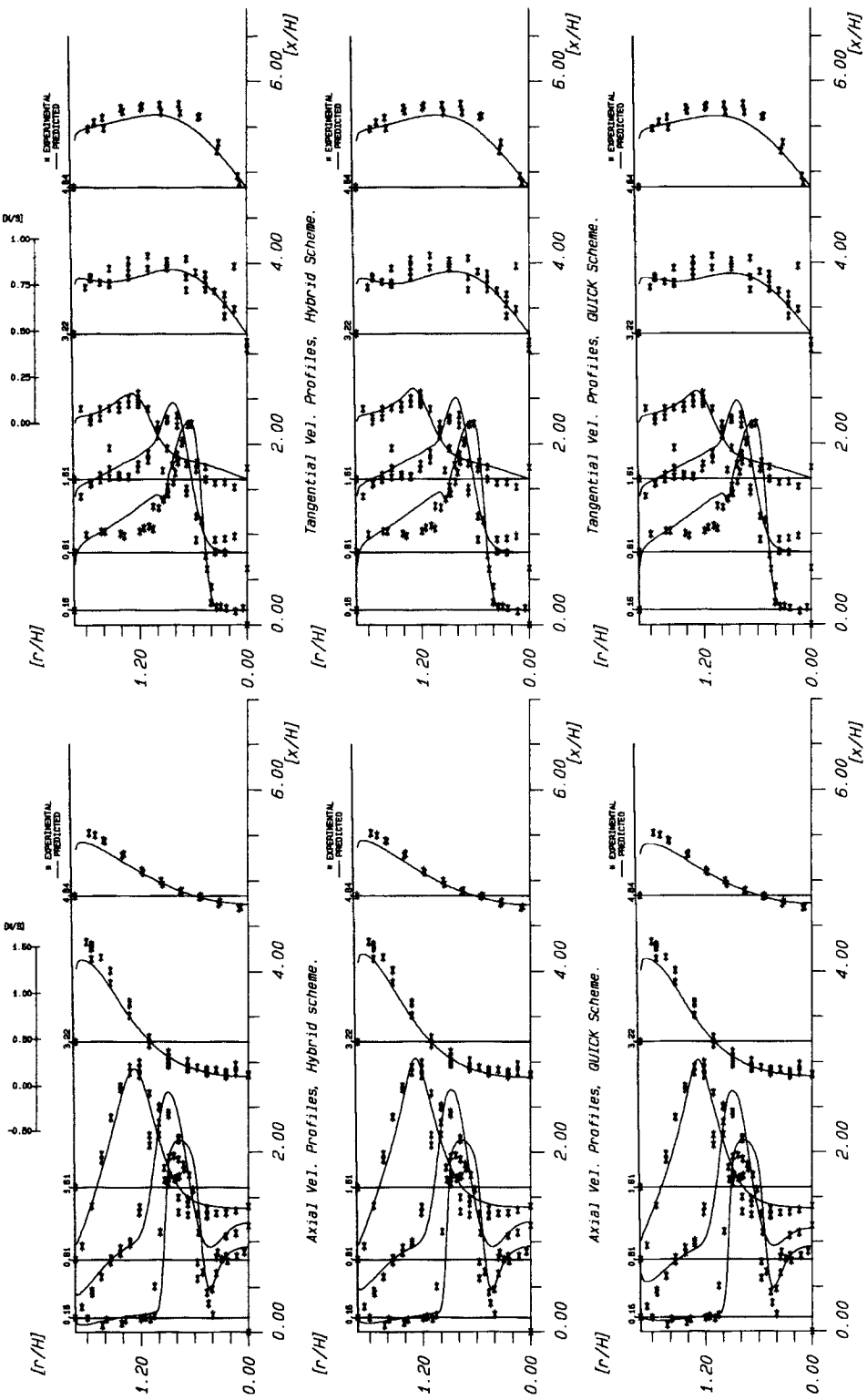

Figure 11. Comparison of axial (left) and tangential (right) velocity profiles with Roback/Johnson experimental data; 154 × 150 grid

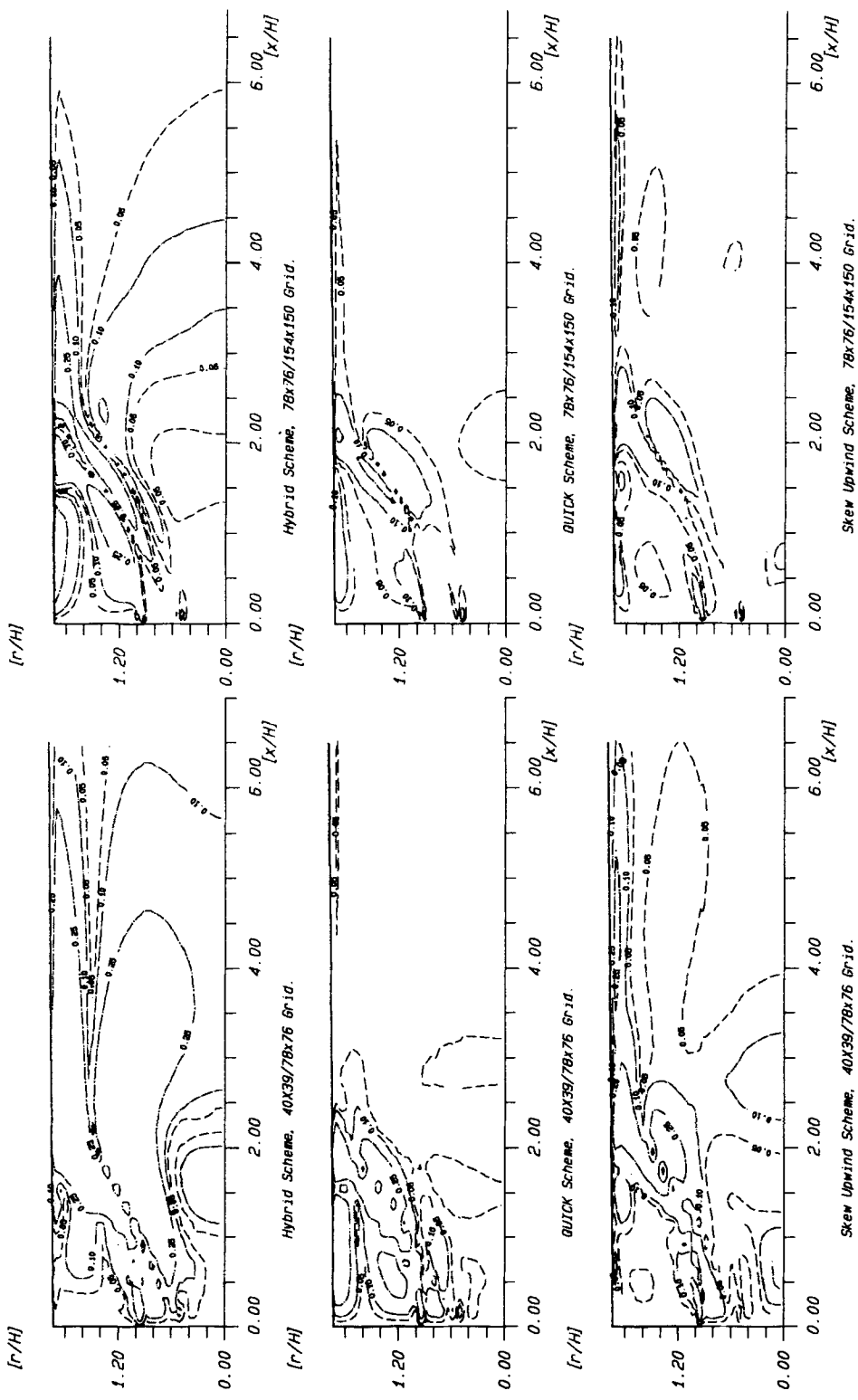

Figure 12. Comparison of error estimates for axial velocity: left, $40 \times 39/78 \times 76$ grids; right, $78 \times 76/154 \times 150$ grids

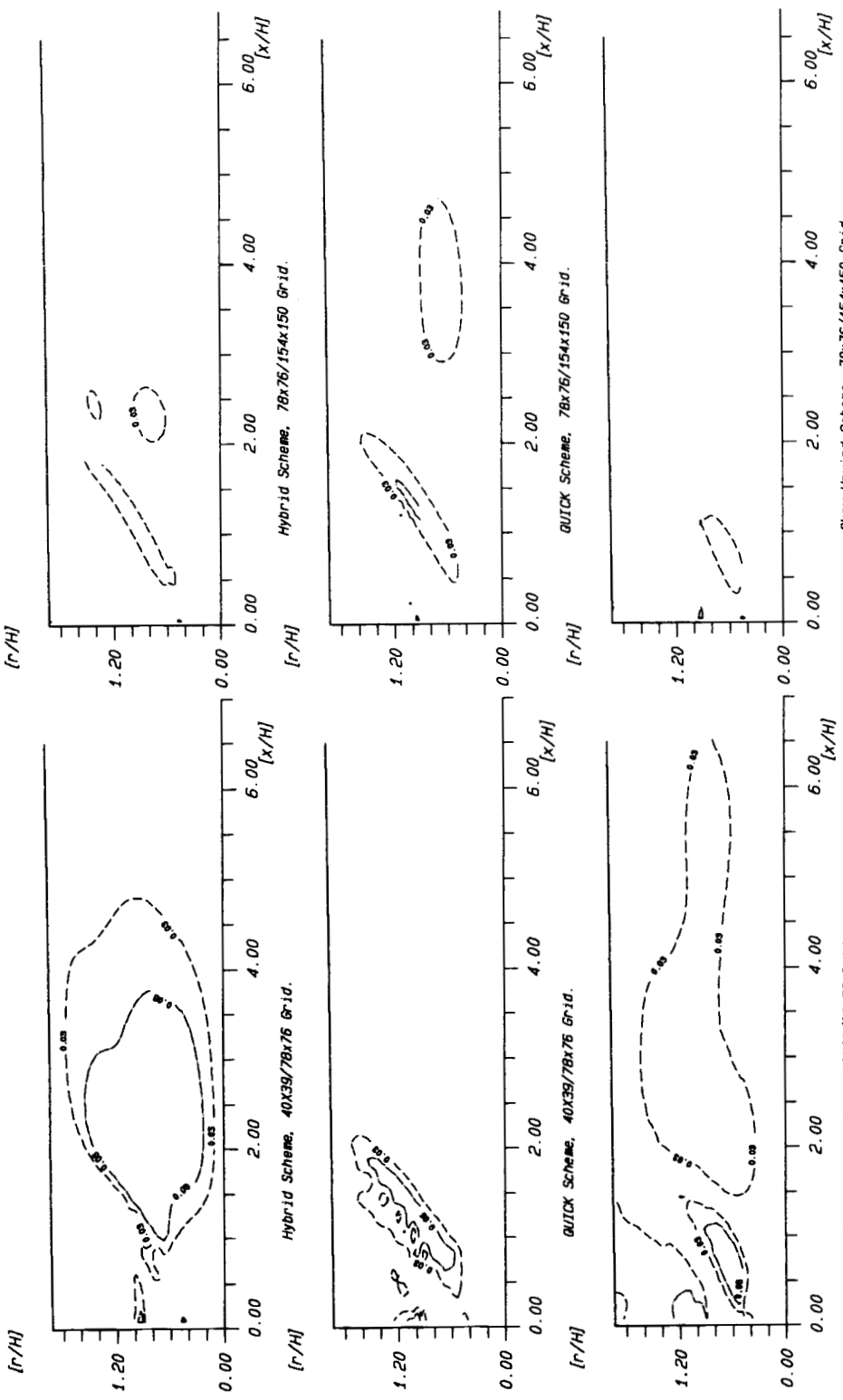

Figure 13. Comparison of error estimates for tangential velocity: left, $40 \times 39/78 \times 76$ grids; right, $78 \times 76/154 \times 150$ grids

practical applications. The form of the predicted turbulence intensity profiles in the bottom panel of Figure 10 is essentially correct, but the level is too high.

The influence of the different formulations of the convective terms and the influence of the nodalization are shown as comparisons of error estimates for axial and tangential velocities in Figures 12 and 13 respectively, calculated as in the laminar flow case. On the left-hand side are the comparisons of the coarser grids and on the right-hand side the finer grids. The panels are in order from top to bottom and provide results calculated with hybrid, QUICK and skew upwind differencing schemes respectively. As expected, the regions with larger relative differences are concentrated in the shear regions between the two recirculation zones and in the wall–jet region downstream, but also upstream of the wall reattachment point (Figure 12). The differences are markedly larger for the hybrid scheme than for the other two differencing schemes. In Figure 12 the cross-hatched areas indicate relative differences larger than 25% and the hatched areas 10%. For the QUICK and skew upwind schemes, 10% error fields still exist at such relatively fine grids as 78×76 and 154×150; see the right side of Figure 12. Grid independence thus requires even finer grids, and for the hybrid scheme obviously much finer. The difference levels for the tangential velocity are essentially lower (normalized with an average tangential velocity calculated via the swirl number); the hatched area indicates the 5% level in Figure 13.

In the present computations the skew upwind scheme turned out to be the most efficient, for axial as well as tangential velocities. This can be expected, since the high-shear region between the recirculation zones is at an angle of approximately 45° with the co-ordinate system used. Evidently the source terms in the tangential veloctiy equation are important in this case, with a substantial radial velocity component (see Table I).

5. CONCLUSIONS

Flow predictions were performed of two different confined swirling flows with internal recirculation zones. The convection terms in the elliptic governing equations, equation (1), have been discretized using three different schemes: hybrid, quadratic upwind interpolation and skew upwind differencing. For each flow case, calculations were performed with these schemes using a coarse and two finer numerical grids.

The predictions showed that the proper choice of inlet conditions is very important. In swirling flow the rotating motion of the flow forces a radial velocity component to be present in the flow already at the inlet plane, i.e. after the swirler. In order to have a complete set of data for predictions, this component should also be measured in all experimental studies of such flows. If it is not available, an estimate of this component has to be made from streamfunction calculations and has to be used as initial data.

The laminar swirling flow of Bornstein and Escudier[26] was well predicted when account was taken of the estimated radial velocity component at the chosen inlet plane. The QUICK and skew upwind schemes also predicted the main features of the internal recirculation zone with the coarser grid. With the finest grid the QUICK and skew upwind schemes were very close to Bornstein and Escudier's measured velocity profiles. The skew upwind scheme approached grid independence faster than QUICK, since the flux-blending factors could also be kept at 1·0 with the finest grid.

In the turbulent low-swirl flow of Roback and Johnson[27] the mean flow properties, i.e. axial and tangential velocities, were very well predicted in almost all cases, also with the coarser grid used. However, a close look at the predicted profiles in the region where the forward flow is diverted around the central recirculation zone revealed that the finer grid and higher-order differencing schemes perform better in this region. In this test case the skew upwind scheme was

slightly better than the QUICK and hybrid schemes and also approached grid independence earlier. The hybrid scheme required a finer grid than the skew upwind and QUICK schemes to reach grid independence, in this case finer than 154×150.

It is clear that extreme care must be taken when predicting swirling flows with internal recirculation zones. Fine grids had to be used together with differencing schemes that minimize the effects of numerical diffusion. From the results presented here, it can be concluded that the skew upwind scheme should be the best choice and reaches grid independence faster than the hybrid and QUICK schemes for these types of flows. For flows with lower swirl numbers, i.e. up to 0·5, the k–ε model results in sufficiently good predictions of the mean flow properties, at least sufficient for many practical applications of the results.

REFERENCES

1. T. B. Benjamin, 'Theory of vortex breakdown phenomena', *J. Fluid Mech.*, **14**, 593–629 (1962).
2. T. B. Benjamin, 'Significance of the vortex breakdown phenomenon', *J. Basic Eng.*, 518–524 (1965).
3. J. H. Faler and S. Leibovich, 'Disrupted states of vortex flow and vortex breakdown', *Phys. Fluids*, **20**, 1385–1400 (1977).
4. J. H. Faler and S. Leibovich, 'An experimental map of the internal structure of a vortex breakdown', *J. Fluid Mech.*, **86**, 313–335 (1978).
5. S. Leibovich, 'Vortex stability and breakdown: survey and extension', *AIAA J.*, **22**, 1192–1206 (1984).
6. M. P. Escudier and N. Zehnder, 'Vortex flow regimes', *J. Fluid Mech.*, **115**, 105–121 (1982).
7. D. Wennerberg, 'Prediction of pulverized coal and peat flames', *Combust. Sci. Technol.*, **58**, 25–41 (1988).
8. M. A. Leschziner, 'Practical evaluation of three finite difference schemes for the computation of steady-state recirculating flows', *Comput. Methods Appl. Mech. Eng.*, **23**, 293–312 (1980).
9. M. A. Leschziner and W. Rodi, 'Calculation of annular and twin parallel jets using various discretization schemes and turbulence model variations', *J. Fluids Eng.*, **103**, 352–360 (1981).
10. M. A. R. Sharif and A. A. Busnaina, 'Assessment of finite difference approximations in the simulation of practical flow problems', *AIAA Paper 86-0216, AIAA 24th Aerospace Meeting*, January 1986.
11. M. Patel, M. Gross, N. C. Markatos and R. C. H. Mace, 'An evaluation of eleven discretization schemes for predicting elliptic flow and heat transfer in supersonic jets', *Int. J. Heat Mass Transfer*, **30**, 1907–1925 (1987).
12. S. A. Syed, L. M. Chiappetta and A. D. Gosman, 'Error reduction program—final report', *NASA CR-174776*, 1985.
13. G. J. Sturgess and S. A. Syed, 'Calculation of confined swirling flows', *AIAA Paper 85-0060, AIAA 23rd Aerospace Meeting*, January 1985.
14. M. Nikjooy, 'On the modelling of non-reactive and reactive turbulent combustor flows', *Ph.D. Thesis*, Arizona State University, 1987.
15. D. L. Rhode and S. T. Stowers, 'Turbulence model assessment for the confined mixing of co-swirling concentric jets', *AIAA Paper 85-1269, AIAA 21st Propulsion Conf.*, 1985.
16. R. Weber, F. Boysan, J. Swithenbank and P. A. Roberts, 'Computations of near field aerodynamics of swirling expanding flows', *Proc. 21st Symp. (Int.) on Combustion*, The Combustion Institute, Pittsburgh, 1986, pp. 1435–1443.
17. E. E. Khalil, *Modelling of Furnace and Combustor Flows*, Abacus Press, Kent, U.K., 1984.
18. G. D. Raithby, 'Skew upstream differencing schemes for problems involving fluid flow', *Comput. Methods Appl. Mech. Eng.*, **9**, 153–164 (1976).
19. M. Peric, R. Kessler and G. Scheurer, 'Comparison of finite-volume numerical methods with staggered and collocated grids', *Comput. Fluids*, **16**, 389–403 (1988).
20. B. P. Leonard, 'A stable and accurate convective modelling procedure based on quadratic upstream interpolation', *Comput. Methods Appl. Mech. Eng.*, **19**, 59–98 (1979).
21. A. Pollard and A. L.-W. Siu, 'The calculation of some laminar flows using various discretisation schemes', *Comput. Methods Appl. Mech. Eng.*, **35**, 293–313 (1982).
22. W. Shyy, 'A numerical study of annular dump diffuser flows', *Comput. Methods Appl. Mech. Eng.*, **53**, 47–65 (1985).
23. S. V. Patankar, *Numerical Heat Transfer and Fluid Flow*, McGraw-Hill, New York, 1980.
24. H. L. Stone, 'Iterative solution of implicit approximations of multi-dimensional partial differential equations', *SIAM J. Numer. Anal.*, **5**, 530–558 (1968).
25. D. G. Sloan, P. J. Smith and L. D. Smoot, 'Modeling of swirl in turbulent flow systems', *Prog. Energy Combust. Sci.*, **12**, 163–250 (1986).
26. J. Bornstein and M. P. Escudier, 'LDA measurements within a vortex-breakdown bubble', *Int. Symp. on Applications of LDA to Fluid Mechanics*, Lisbon, 1982, Paper 10.3.
27. R. Roback and B. V. Johnson, 'Mass and momentum turbulent transport experiments with confined swirling co-axial jets', *NASA CR-168252*, 1983.